Title

Observation of pi+pi-pi+pi- photoproduction in ultraperipheral heavy-ion collisions at sqrt sNN = 200 GeV at the STAR detector

Author

Abelev, Betty

Publication Date

2010-02-25

Observation of pi^+pi^-pi^+pi^- photoproduction in ultraperipheral heavy-ion collisions at sqrt(s_NN) = 200 GeV at the STAR detector

B.I.Abelev
(STARCollaboration)
February 25, 2010

This work was supported by the Director, Office of Science, Office of Nuclear Science of the U.S. Department of Energy under Contract No. DE-AC02-05CH11231.

Observation of $\pi^+\pi^-\pi^+\pi^-$ Photoproduction in Ultra-Peripheral Heavy Ion Collisions at $\sqrt{s_{NN}} = 200$ GeV at the STAR Detector

B. I. Abelev,[8] M. M. Aggarwal,[30] Z. Ahammed,[47] A. V. Alakhverdyants,[17] B. D. Anderson,[18] D. Arkhipkin,[3] G. S. Averichev,[17] J. Balewski,[22] L. S. Barnby,[2] S. Baumgart,[52] D. R. Beavis,[3] R. Bellwied,[50] F. Benedosso,[27] M. J. Betancourt,[22] R. R. Betts,[8] A. Bhasin,[16] A. K. Bhati,[30] H. Bichsel,[49] J. Bielcik,[10] J. Bielcikova,[11] B. Biritz,[6] L. C. Bland,[3] B. E. Bonner,[36] J. Bouchet,[18] E. Braidot,[27] A. V. Brandin,[25] A. Bridgeman,[1] E. Bruna,[52] S. Bueltmann,[29] I. Bunzarov,[17] T. P. Burton,[2] X. Z. Cai,[40] H. Caines,[52] M. Calderón de la Barca Sánchez,[5] O. Catu,[52] D. Cebra,[5] R. Cendejas,[6] M. C. Cervantes,[42] Z. Chajecki,[28] P. Chaloupka,[11] S. Chattopadhyay,[47] H. F. Chen,[38] J. H. Chen,[40] J. Y. Chen,[51] J. Cheng,[44] M. Cherney,[9] A. Chikanian,[52] K. E. Choi,[34] W. Christie,[3] P. Chung,[11] S. U. Chung,[3] R. F. Clarke,[42] M. J. M. Codrington,[42] R. Corliss,[22] J. G. Cramer,[49] H. J. Crawford,[4] D. Das,[5] S. Dash,[13] A. Davila Leyva,[43] L. C. De Silva,[50] R. R. Debbe,[3] T. G. Dedovich,[17] M. DePhillips,[3] A. A. Derevschikov,[32] R. Derradi de Souza,[7] L. Didenko,[3] P. Djawotho,[42] S. M. Dogra,[16] X. Dong,[21] J. L. Drachenberg,[42] J. E. Draper,[5] J. C. Dunlop,[3] M. R. Dutta Mazumdar,[47] L. G. Efimov,[17] E. Elhalhuli,[2] M. Elnimr,[50] J. Engelage,[4] G. Eppley,[36] B. Erazmus,[41] M. Estienne,[41] L. Eun,[31] O. Evdokimov,[8] P. Fachini,[3] R. Fatemi,[19] J. Fedorisin,[17] R. G. Fersch,[19] P. Filip,[17] E. Finch,[52] V. Fine,[3] Y. Fisyak,[3] C. A. Gagliardi,[42] D. R. Gangadharan,[6] M. S. Ganti,[47] E. J. Garcia-Solis,[8] A. Geromitsos,[41] F. Geurts,[36] V. Ghazikhanian,[6] P. Ghosh,[47] Y. N. Gorbunov,[9] A. Gordon,[3] O. Grebenyuk,[21] D. Grosnick,[46] B. Grube,[34] S. M. Guertin,[6] A. Gupta,[16] N. Gupta,[16] W. Guryn,[3] B. Haag,[5] T. J. Hallman,[3] A. Hamed,[42] L-X. Han,[40] J. W. Harris,[52] J. P. Hays-Wehle,[22] M. Heinz,[52] S. Heppelmann,[31] A. Hirsch,[33] E. Hjort,[21] A. M. Hoffman,[22] G. W. Hoffmann,[43] D. J. Hofman,[8] R. S. Hollis,[8] H. Z. Huang,[6] T. J. Humanic,[28] L. Huo,[42] G. Igo,[6] A. Iordanova,[8] P. Jacobs,[21] W. W. Jacobs,[15] P. Jakl,[11] C. Jena,[13] F. Jin,[40] C. L. Jones,[22] P. G. Jones,[2] J. Joseph,[18] E. G. Judd,[4] S. Kabana,[41] K. Kajimoto,[43] K. Kang,[44] J. Kapitan,[11] K. Kauder,[8] D. Keane,[18] A. Kechechyan,[17] D. Kettler,[49] D. P. Kikola,[21] J. Kiryluk,[21] A. Kisiel,[48] S. R. Klein,[21] A. G. Knospe,[52] A. Kocoloski,[22] D. D. Koetke,[46] T. Kollegger,[12] J. Konzer,[33] M. Kopytine,[18] I. Koralt,[29] W. Korsch,[19] L. Kotchenda,[25] V. Kouchpil,[11] P. Kravtsov,[25] K. Krueger,[1] M. Krus,[10] L. Kumar,[30] P. Kurnadi,[6] M. A. C. Lamont,[3] J. M. Landgraf,[3] S. LaPointe,[50] J. Lauret,[3] A. Lebedev,[3] R. Lednicky,[17] C-H. Lee,[34] J. H. Lee,[3] W. Leight,[22] M. J. LeVine,[3] C. Li,[38] L. Li,[43] N. Li,[51] W. Li,[40] X. Li,[33] X. Li,[39] Y. Li,[44] Z. Li,[51] G. Lin,[52] S. J. Lindenbaum,[26] M. A. Lisa,[28] F. Liu,[51] H. Liu,[5] J. Liu,[36] T. Ljubicic,[3] W. J. Llope,[36] R. S. Longacre,[3] W. A. Love,[3] Y. Lu,[38] G. L. Ma,[40] Y. G. Ma,[40] D. P. Mahapatra,[13] R. Majka,[52] O. I. Mall,[5] L. K. Mangotra,[16] R. Manweiler,[46] S. Margetis,[18] C. Markert,[43] H. Masui,[21] H. S. Matis,[21] Yu. A. Matulenko,[32] D. McDonald,[36] T. S. McShane,[9] A. Meschanin,[32] R. Milner,[22] N. G. Minaev,[32] S. Mioduszewski,[42] A. Mischke,[27] M. K. Mitrovski,[12] B. Mohanty,[47] M. M. Mondal,[47] D. A. Morozov,[32] M. G. Munhoz,[37] B. K. Nandi,[14] C. Nattrass,[52] T. K. Nayak,[47] J. M. Nelson,[2] P. K. Netrakanti,[33] M. J. Ng,[4] L. V. Nogach,[32] S. B. Nurushev,[32] G. Odyniec,[21] A. Ogawa,[3] H. Okada,[3] V. Okorokov,[25] D. Olson,[21] M. Pachr,[10] B. S. Page,[15] S. K. Pal,[47] Y. Pandit,[18] Y. Panebratsev,[17] T. Pawlak,[48] T. Peitzmann,[27] V. Perevoztchikov,[3] C. Perkins,[4] W. Peryt,[48] S. C. Phatak,[13] P. Pile,[3] M. Planinic,[53] M. A. Ploskon,[21] J. Pluta,[48] D. Plyku,[29] N. Poljak,[53] A. M. Poskanzer,[21] B. V. K. S. Potukuchi,[16] C. B. Powell,[21] D. Prindle,[49] C. Pruneau,[50] N. K. Pruthi,[30] P. R. Pujahari,[14] J. Putschke,[52] R. Raniwala,[35] S. Raniwala,[35] R. L. Ray,[43] R. Redwine,[22] R. Reed,[5] J. M. Rehberg,[12] H. G. Ritter,[21] J. B. Roberts,[36] O. V. Rogachevskiy,[17] J. L. Romero,[5] A. Rose,[21] C. Roy,[41] L. Ruan,[3] M. J. Russcher,[27] R. Sahoo,[41] S. Sakai,[6] I. Sakrejda,[21] T. Sakuma,[22] S. Salur,[5] J. Sandweiss,[52] E. Sangaline,[5] J. Schambach,[43] R. P. Scharenberg,[33] N. Schmitz,[23] T. R. Schuster,[12] J. Seele,[22] J. Seger,[9] I. Selyuzhenkov,[15] P. Seyboth,[23] E. Shahaliev,[17] M. Shao,[38] M. Sharma,[50] S. S. Shi,[51] E. P. Sichtermann,[21] F. Simon,[23] R. N. Singaraju,[47] M. J. Skoby,[33] N. Smirnov,[52] P. Sorensen,[3] J. Sowinski,[15] H. M. Spinka,[1] B. Srivastava,[33] T. D. S. Stanislaus,[46] D. Staszak,[6] J. R. Stevens,[15] R. Stock,[12] M. Strikhanov,[25] B. Stringfellow,[33] A. A. P. Suaide,[37] M. C. Suarez,[8] N. L. Subba,[18] M. Sumbera,[11] X. M. Sun,[21] Y. Sun,[38] Z. Sun,[20] B. Surrow,[22] T. J. M. Symons,[21] A. Szanto de Toledo,[37] J. Takahashi,[7] A. H. Tang,[3] Z. Tang,[38] L. H. Tarini,[50] T. Tarnowsky,[24] D. Thein,[43] J. H. Thomas,[21] J. Tian,[40] A. R. Timmins,[50] S. Timoshenko,[25] D. Tlusty,[11] M. Tokarev,[17] T. A. Trainor,[49] V. N. Tram,[21] S. Trentalange,[6] R. E. Tribble,[42] O. D. Tsai,[6] J. Ulery,[33] T. Ullrich,[3] D. G. Underwood,[1] G. Van Buren,[3] G. van Nieuwenhuizen,[22] J. A. Vanfossen, Jr.,[18] R. Varma,[14] G. M. S. Vasconcelos,[7] A. N. Vasiliev,[32] F. Videbaek,[3] Y. P. Viyogi,[47] S. Vokal,[17] S. A. Voloshin,[50] M. Wada,[43] M. Walker,[22] F. Wang,[33] G. Wang,[6] H. Wang,[24] J. S. Wang,[20] Q. Wang,[33] X. Wang,[44] X. L. Wang,[38] Y. Wang,[44] G. Webb,[19] J. C. Webb,[3] G. D. Westfall,[24] C. Whitten Jr.,[6] H. Wieman,[21] E. Wingfield,[43] S. W. Wissink,[15] R. Witt,[45] Y. Wu,[51] W. Xie,[33] N. Xu,[21] Q. H. Xu,[39] W. Xu,[6] Y. Xu,[38] Z. Xu,[3] L. Xue,[40] Y. Yang,[20] P. Yepes,[36] K. Yip,[3] I-K. Yoo,[34] Q. Yue,[44]

M. Zawisza,[48] H. Zbroszczyk,[48] W. Zhan,[20] S. Zhang,[40] W. M. Zhang,[18] X. P. Zhang,[21] Y. Zhang,[21] Z. P. Zhang,[38] J. Zhao,[40] C. Zhong,[40] J. Zhou,[36] W. Zhou,[39] X. Zhu,[44] Y. H. Zhu,[40] R. Zoulkarneev,[17] and Y. Zoulkarneeva[17]
(STAR Collaboration)

[1]*Argonne National Laboratory, Argonne, Illinois 60439, USA*
[2]*University of Birmingham, Birmingham, United Kingdom*
[3]*Brookhaven National Laboratory, Upton, New York 11973, USA*
[4]*University of California, Berkeley, California 94720, USA*
[5]*University of California, Davis, California 95616, USA*
[6]*University of California, Los Angeles, California 90095, USA*
[7]*Universidade Estadual de Campinas, Sao Paulo, Brazil*
[8]*University of Illinois at Chicago, Chicago, Illinois 60607, USA*
[9]*Creighton University, Omaha, Nebraska 68178, USA*
[10]*Czech Technical University in Prague, FNSPE, Prague, 115 19, Czech Republic*
[11]*Nuclear Physics Institute AS CR, 250 68 Řež/Prague, Czech Republic*
[12]*University of Frankfurt, Frankfurt, Germany*
[13]*Institute of Physics, Bhubaneswar 751005, India*
[14]*Indian Institute of Technology, Mumbai, India*
[15]*Indiana University, Bloomington, Indiana 47408, USA*
[16]*University of Jammu, Jammu 180001, India*
[17]*Joint Institute for Nuclear Research, Dubna, 141 980, Russia*
[18]*Kent State University, Kent, Ohio 44242, USA*
[19]*University of Kentucky, Lexington, Kentucky, 40506-0055, USA*
[20]*Institute of Modern Physics, Lanzhou, China*
[21]*Lawrence Berkeley National Laboratory, Berkeley, California 94720, USA*
[22]*Massachusetts Institute of Technology, Cambridge, MA 02139-4307, USA*
[23]*Max-Planck-Institut für Physik, Munich, Germany*
[24]*Michigan State University, East Lansing, Michigan 48824, USA*
[25]*Moscow Engineering Physics Institute, Moscow Russia*
[26]*City College of New York, New York City, New York 10031, USA*
[27]*NIKHEF and Utrecht University, Amsterdam, The Netherlands*
[28]*Ohio State University, Columbus, Ohio 43210, USA*
[29]*Old Dominion University, Norfolk, VA, 23529, USA*
[30]*Panjab University, Chandigarh 160014, India*
[31]*Pennsylvania State University, University Park, Pennsylvania 16802, USA*
[32]*Institute of High Energy Physics, Protvino, Russia*
[33]*Purdue University, West Lafayette, Indiana 47907, USA*
[34]*Pusan National University, Pusan, Republic of Korea*
[35]*University of Rajasthan, Jaipur 302004, India*
[36]*Rice University, Houston, Texas 77251, USA*
[37]*Universidade de Sao Paulo, Sao Paulo, Brazil*
[38]*University of Science & Technology of China, Hefei 230026, China*
[39]*Shandong University, Jinan, Shandong 250100, China*
[40]*Shanghai Institute of Applied Physics, Shanghai 201800, China*
[41]*SUBATECH, Nantes, France*
[42]*Texas A&M University, College Station, Texas 77843, USA*
[43]*University of Texas, Austin, Texas 78712, USA*
[44]*Tsinghua University, Beijing 100084, China*
[45]*United States Naval Academy, Annapolis, MD 21402, USA*
[46]*Valparaiso University, Valparaiso, Indiana 46383, USA*
[47]*Variable Energy Cyclotron Centre, Kolkata 700064, India*
[48]*Warsaw University of Technology, Warsaw, Poland*
[49]*University of Washington, Seattle, Washington 98195, USA*
[50]*Wayne State University, Detroit, Michigan 48201, USA*
[51]*Institute of Particle Physics, CCNU (HZNU), Wuhan 430079, China*
[52]*Yale University, New Haven, Connecticut 06520, USA*
[53]*University of Zagreb, Zagreb, HR-10002, Croatia*

(Dated: February 25, 2010)

We present a measurement of $\pi^+\pi^-\pi^+\pi^-$ photonuclear production in ultra-peripheral Au-Au collisions at $\sqrt{s_{NN}} = 200$ GeV from the STAR experiment. The $\pi^+\pi^-\pi^+\pi^-$ final states are observed at low transverse momentum and are accompanied by mutual nuclear excitation of the beam particles. The strong enhancement of the production cross section at low transverse momentum is consistent with coherent photoproduction. The $\pi^+\pi^-\pi^+\pi^-$ invariant mass spectrum of the coherent events exhibits a broad peak around 1540 ± 40 MeV/c^2 with a width of 570 ± 60 MeV/c^2, in agreement with the photoproduction data for the $\rho^0(1700)$. We do not observe a corresponding peak in the $\pi^+\pi^-$ final state and measure an upper limit for the ratio of the branching fractions of the $\rho^0(1700)$ to $\pi^+\pi^-$ and $\pi^+\pi^-\pi^+\pi^-$ of 2.5 % at 90 % confidence level. The ratio of $\rho^0(1700)$ and $\rho^0(770)$ coherent production cross sections is measured to be $13.4 \pm 0.8_{\text{stat.}} \pm 4.4_{\text{syst.}}$%.

PACS numbers: 25.20.Lj, 13.60.-r

I. INTRODUCTION

The electromagnetic field of a relativistic heavy nucleus can be approximated by a flux of quasi-real virtual photons using the Weizsäcker-Williams approach [1]. Because the number of photons grows with the square of the nuclear charge, fast moving heavy ions generate intense photon fluxes. Relativistic heavy ions can thus be used as photon sources or targets. Due to the long range of the electromagnetic interactions, they can be separated from the hadronic interactions by requiring impact parameter b larger than the sum of the nuclear radii R_A of the beam particles. These so-called ultra-peripheral heavy ion collisions (UPCs) allow us to study photonuclear effects as well as photon-photon interactions [2].

A typical high-energy photonuclear reaction in UPCs is the production of vector mesons. In this process the virtual photon, radiated by the "emitter" nucleus, fluctuates into a virtual $q\overline{q}$-pair, which scatters elastically off the "target" nucleus, thus producing a real vector meson. The scattering can be described in terms of soft Pomeron exchange. The cross section for vector meson production depends on how the virtual $q\overline{q}$-pair couples to the target nucleus. This is mainly determined by the transverse momentum p_T of the produced meson. For small transverse momenta of the order of $p_T \lesssim \hbar/R_A$ the $q\overline{q}$-pair couples coherently to the entire nucleus. This leads to large cross sections which depend on the nuclear form factor $F(t)$, where t is the square of the momentum transfer to the target nucleus. For larger transverse momenta the $q\overline{q}$-pair couples to the individual nucleons in the target nucleus. This "incoherent" scattering has a smaller cross section that scales approximately with the mass number A modulo corrections for nuclear absorption of the meson.

Due to the intense photon flux in UPCs, it is possible that vector meson production is accompanied by Coulomb excitation of the beam particles. The excited ions mostly decay via the emission of neutrons [3] which is a distinctive event signature that is utilized in the trigger decision. To lowest order, events with mutual nuclear dissociation are described by three-photon exchange (see Fig. 1): one photon to produce the vector meson and two photons to excite the nuclei. All three photon exchanges are in good approximation independent, so that the cross section for the production of a vector meson V accompanied by mutual nuclear dissociation can be factorized [3]:

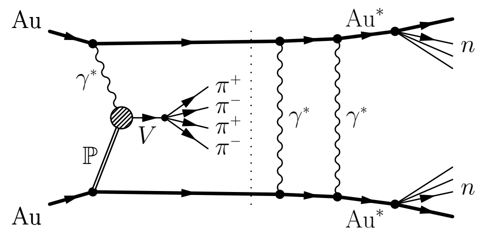

FIG. 1: Schematic view of the photonuclear production of a vector meson V in an ultra-peripheral Au-Au collision and its subsequent decay into four charged pions. The meson production in the fusion processes of photon γ^* and Pomeron $\mathbb{P}$ is accompanied by mutual Coulomb excitation of the beam ions. The processes are independent as indicated by the dotted line.

$$\sigma_{V,\,xn\,xn} = \int \mathrm{d}^2 b\,[1 - P_{\text{had}}(b)] \cdot P_V(b) \cdot P_{xn,1}(b) \cdot P_{xn,2}(b), \tag{1}$$

where $P_{\text{had}}(b)$ is the probability for hadronic interaction, $P_V(b)$ the probability to produce a vector meson V, and $P_{xn,i}(b)$ the probability that nucleus i emits x neutrons. Compared to exclusive photonuclear vector meson production, reactions with mutual Coulomb excitation have smaller median impact parameters.

The PDG currently lists two excited ρ^0 states, the $\rho^0(1450)$ and the $\rho^0(1700)$, which are seen in various production modes and decay channels including two- and four-pion final states [4]. The nature of these states is still an open question, because their decay patterns do not match quark model predictions [5]. Little data exist on high-energy photoproduction of excited ρ^0 states in the four-pion decay channel. Most of them are from photon-proton or photon-deuteron fixed target experiments at photon energies in the range from 2.8 to 18 GeV [6–9]. The OMEGA spectrometer measured photoproduction on proton targets at energies E_γ of up to 70 GeV [10]. The heaviest target nucleus used so far to study diffractive two- and four-pion photoproduction was carbon with photon energies between 50 and 200 GeV [11]. These experiments observe a broad structure in the four-pion invariant mass distribution at masses ranging from 1430 ± 50 MeV/c^2 [6] to 1570 ± 60 MeV/c^2 [8] and with widths between 340 ± 60 MeV/c^2 [8] and 850 ± 200 MeV/c^2 [7] that the PDG assigns to the $\rho^0(1700)$. However, data indicate that the peak might consist of two resonances [9].

We will use the symbol ρ' to designate this structure in the rest of the text.

The measurements presented in this paper extend the four-pion photoproduction data to fixed target equivalent photon energies of up to 320 GeV as well as to heavy target nuclei. This represents the first measurement of four-prong production in ultra-peripheral heavy ion collisions complementing the pioneering work on e^+e^-, $\rho^0(770)$, and J/ψ production in UPCs at STAR [12–15] and PHENIX [16].

There are at least three models for the production of $\rho^0(770)$ mesons in ultra-peripheral collisions: The model of Klein and Nystrand (KN) [17] employs the Vector Dominance Model (VDM) to describe the virtual photon and a classical mechanical approach for the scattering on the target nucleus, using results from $\gamma\, p \to \rho^0(770)\, p$ experiments. The Frankfurt, Strikman, and Zhalov (FSZ) model [18] is based on a generalized VDM for the virtual photon and a QCD Gribov-Glauber approach for the scattering. The model of Gonçalves and Machado (GM) [19] employs a QCD color dipole approach that takes into account nuclear effects and parton saturation phenomena. The KN model agrees best with the available data on $\rho^0(770)$ production, the FSZ and in particular the GM model overestimate the $\rho^0(770)$ production cross section [14]. Only the FSZ calculations make predictions about the production of exited ρ^0 states in UPCs.

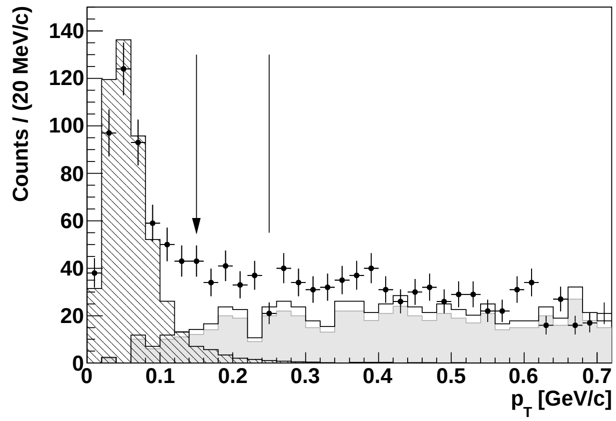

FIG. 2: Distribution of the $\pi^+\pi^-\pi^+\pi^-$ transverse momentum $p_T = \left|\sum_{i=1}^{4} \vec{p}_{T,i}\right|$: The filled circles are the measured points with the statistical errors. The hatched filled histogram shows the expected distribution from simulation of coherent photoproduction (cf. section III). The strong enhancement at low transverse momenta is due to coherently produced $\pi^+\pi^-\pi^+\pi^-$. This unique signature is used in the event selection which requires $p_T < 150$ MeV/c (arrow). The remaining background is estimated from $+2$ or -2 charged four-prong combinations, by normalizing (factor $= 1.186 \pm 0.054$) their p_T distribution (gray filled histogram) to that of the neutral four-prongs in the region of $p_T > 250$ MeV/c (vertical line) yielding the unfilled histogram (see section IV).

II. EXPERIMENTAL SETUP AND DATA SELECTION

The analysis is based on $1.9 \cdot 10^6$ events taken with the STAR experiment at the Relativistic Heavy Ion Collider (RHIC) in Au-Au collisions at $\sqrt{s_{NN}} = 200$ GeV during the year 2007 run. The Solenoidal Tracker at RHIC (STAR) experiment uses a large cylindrical Time Projection Chamber (TPC) [20] with 2 m radius and 4.2 m length, operated in a 0.5 T solenoidal magnetic field, to reconstruct charged tracks.

Two detector systems are used for triggering: the Central Trigger Barrel (CTB) [21], which is an array of 240 plastic scintillator slats around the TPC that allows us to trigger on charged particle multiplicities, and the two Zero Degree Calorimeters (ZDCs) [22], which are located at ±18 m from the interaction point. The ZDCs have an acceptance close to unity for neutrons originating from nuclear dissociation of the beam ions. In the trigger, these neutrons are used to tag UPC events by requiring coincident hits in both ZDCs with amplitudes corresponding to less than about 7 to 10 neutrons. The ADC sum of all CTB slats is restricted to a range equivalent to a hit multiplicity between about 2 and 40 minimum ionizing particles. In order to enrich events at central rapidities, events with hits above the minimum ionizing particle threshold in the large-tile Beam-Beam Counters (BBCs) [23], which cover $2.1 < |\eta| < 3.6$, are vetoed.

In the offline analysis two- and four-prong data sets are selected. Four-prong events are required to have exactly four tracks with zero net charge in the TPC that form a common (primary) vertex. Because the STAR TPC has a drift time of about 36 µsec, any charged tracks produced within a time window of ±36 µsec around the triggered collision will overlap with the event of interest. Some of these additional tracks come from beam induced background reactions, but, due to the high luminosities reached in the RHIC 2007 run [24], a large percentage is from real heavy ion collisions. In order to account for those out-of-time events and backgrounds up to 86 additional tracks per event, which do not point to the primary vertex, are allowed, but excluded from the analysis. The primary vertex is confined to a cylindrical region of 15 cm radius and 200 cm length centered around the interaction diamond which reduces contaminations from pile-up events and beam-gas interactions. Each of the four-prong tracks is required to have at least 14 out of a maximum possible 45 hits in the TPC. No particle identification is employed in the event selection; all four tracks are assumed to be pions. The distribution of the ionization energy loss dE/dx of the selected tracks in the TPC indicates that contaminations from other particle species are small. The transverse momentum distribution of the $\pi^+\pi^-\pi^+\pi^-$ combinations, as shown in Fig. 2, exhibits an enhancement at low p_T, characteristic of coherent production. Coherent events are selected by requiring $p_T < 150$ MeV/c. This cut also suppresses contaminations from peripheral hadronic interactions and from $\pi^+\pi^-\pi^+\pi^- + X$ events, where the X is not reconstructed.

Due to charge conjugation invariance, we expect no $\rho^0(770)\,\rho^0(770)$ component in the diffractively produced $\pi^+\pi^-\pi^+\pi^-$ final state. Possible contributions from $\rho^0(770)$ pair production by two independent photoproduction reactions on the same ion pair are negligible. The KN model predicts a cross section ratio of exclusive photonuclear ρ^0 pair production and exclusive single ρ^0 production of about $1.2 \cdot 10^{-3}$ [17]. For mutual nuclear dissociation of the beam ions the ratio is expected to be of comparable value so that contaminations of the $\pi^+\pi^-\pi^+\pi^-$ sample by this process are at most a few percent. Also $\gamma^*\gamma^* \to \rho^0(770)\,\rho^0(770)$ events contribute below the percent level. Here the cross section ratio for exclusive ρ^0 pair production in two-photon events and exclusive photonuclear $\rho^0(770)$ production was calculated to be $3.2 \cdot 10^{-5}$ for $\rho^0(770)$ pair invariant masses in the range between 1.5 and 1.6 GeV/c^2 [25].

The two-prong selection criteria are very similar and follow the STAR UPC $\rho^0(770)$ analyses [13, 14]. As in the four-prong case, out-of-time events and background are taken into account by allowing up to 36 tracks per event in addition to the two primary TPC tracks. Background from two-photon e^+e^- and photonuclear ω production is negligible [14]. Cosmic ray background is strongly suppressed, due to the ZDC requirement in the trigger.

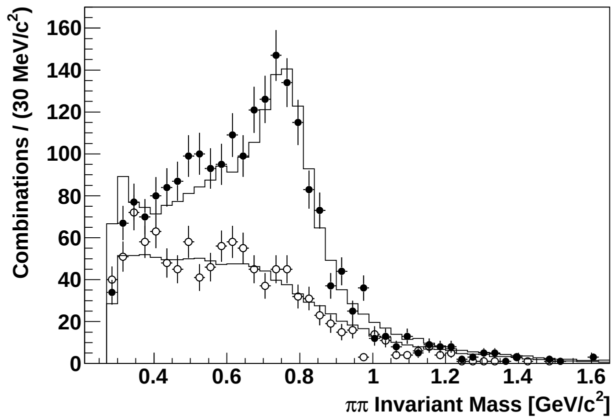

FIG. 3: Invariant Mass distribution of two-pion subsystems: The filled circles show the measured $\pi^+\pi^-$ invariant mass spectrum for the selected four-prong sample (four entries per event) with statistical errors. The open circles represent the mass spectrum of the like-sign pion pairs (two entries per event). The unlike-sign mass distribution exhibits an enhancement with respect to the like-sign pairs in the $\rho^0(770)$ region. The solid line histograms show the prediction from simulation assuming the relative S-wave decay $\rho' \to \rho^0(770)\ f_0(600)$.

III. EFFICIENCY AND ACCEPTANCE CORRECTIONS

Detector efficiency and acceptance are studied using a Monte Carlo event generator based on the KN model [17] which describes coherent vector meson production accompanied by mutual Coulomb excitation in UPCs. In order to reduce model dependence, the acceptance corrections are applied in two stages. Within the detector acceptance of $|y| < 1$, the corrections are calculated using a realistic detector simulation based on GEANT 3 [26]. In a second step, the results are then extrapolated to the full 4π solid angle based on the KN model distributions.

In order to determine the acceptance corrections for the four-prong case, we assume a simple decay model, where an excited ρ^0 meson decays into $\rho^0(770)$ and $f_0(600)$, each in turn decaying into $\pi^+\pi^-$:

$$\rho' \to \rho^0(770)\ f_0(600) \to [\pi^+\pi^-]_{P\text{-wave}}\ [\pi^+\pi^-]_{S\text{-wave}} \tag{2}$$

This decay model is motivated by the fact that the invariant mass spectrum of the unlike-sign two-pion subsystems in the four-prong sample shows an enhancement around the $\rho^0(770)$ mass (cf. Fig. 3). Figure 4 compares the invariant mass spectrum of the lightest $\pi^+\pi^-$ pair with the spectrum of the pair recoiling against it and shows that the four-pion final state consists mainly of a low-mass pion pair accompanied by a $\rho^0(770)$.

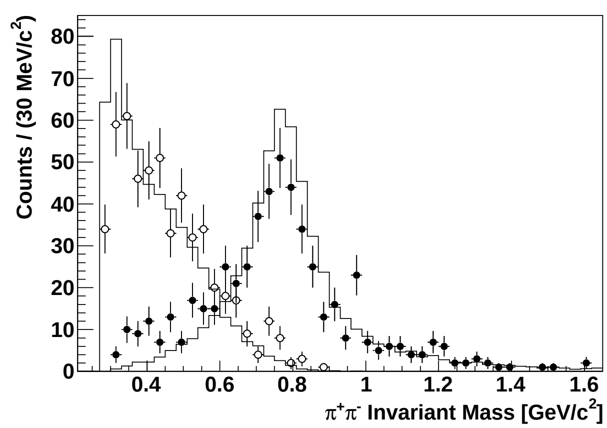

FIG. 4: Invariant Mass distribution of two-pion subsystems: The open circles show the measured invariant mass spectrum of the lightest $\pi^+\pi^-$ pair in the event with the bars indicating the statistical errors. The filled circles represent the invariant mass distribution of the $\pi^+\pi^-$ that is recoiling against the lightest pair. The spectrum exhibits a clear peak in the $\rho^0(770)$ region. The solid line histograms show the prediction from simulation assuming the relative S-wave decay $\rho' \to \rho^0(770)\ f_0(600)$.

In principle, the ρ^0 and f_0 are allowed to be in a relative S- or D-wave, but, due to the low statistics of the data, we are not able to estimate the D-wave parameters. Consequently we only consider S-wave decay. Possible D-wave contributions are well within the estimated systematic error (see section IV).

The angular distribution I that is used to estimate the acceptance corrections for the four-prong sample is parameterized:

$$I \propto \sum_{\epsilon} \sum_{m,m'} {}^{\epsilon}r_{m,m'} \cdot {}^{\epsilon}\mathcal{A}^J_m \cdot {}^{\epsilon}\mathcal{A}^{J*}_{m'}, \tag{3}$$

where ${}^{\epsilon}\mathcal{A}^J_m$ is the amplitude for the decay of a ρ' with spin $J = 1$ and a projection m of J along the quantization axis assuming the model of Eq. (2). ${}^{\epsilon}r_{m,m'}$ represents the spin density matrix elements. The amplitudes are defined in the ρ' rest frame with the z-axis along the beam direction and the y-axis parallel to the production plane normal, $\vec{p}_{\mathrm{beam}} \times \vec{p}_{\rho'}$. Due to the large beam energy and the coherent nature of the production process, this frame coincides approximately with the ρ' helicity frame. Both the amplitudes and the spin density matrix are constructed using eigenstates of the operator Π_y of reflections in the production plane, the so-called reflectivity basis with $\epsilon = \pm 1$ [27]. The sum in Eq. (3) is simplified by assuming s-channel helicity conservation (SCHC) and that the quasi-real photons come with helicities ± 1 only, so that ${}^{-}r_{11} = {}^{+}r_{11}$ are the only non-zero spin density matrix elements. The amplitudes ${}^{\epsilon}\mathcal{A}^J_m$ are factorized:

$${}^{\epsilon}\mathcal{A}^J_m = \Delta_{\rho}(m_{\rho}) \cdot \Delta_{f_0}(m_{f_0}) \cdot {}^{\epsilon}\mathcal{M}^J_m(\theta, \phi; \theta_{\rho}, \phi_{\rho}, \gamma_{\rho}) \tag{4}$$

Here Δ_{ρ,f_0} are the amplitudes for the ρ^0 and f_0 resonance shapes as a function of the invariant masses of the intermediate states m_{ρ,f_0}. For the $\rho^0(770)$ a P-wave Breit-Wigner with mass-dependent width including Blatt-Weisskopf barrier factors is used [28]. The f_0 is modeled by an S-wave Breit-Wigner at 400 MeV/c^2 with a width of 600 MeV/c^2. The decay amplitudes ${}^{\epsilon}\mathcal{M}^J_m$ describe the angular dependence and include relativistic corrections via the Lorentz factor γ_{ρ} of the ρ^0 in the ρ' rest frame (RF) according to [29]. ${}^{\epsilon}\mathcal{M}^J_m$ depends on the angles θ and ϕ of the ρ^0 in the ρ' rest frame as well as on the angles θ_{ρ} and ϕ_{ρ} that describe the orientation of the π^+ from the ρ^0 decay in the ρ^0 helicity rest frame. This frame is defined starting from the ρ' rest frame and has its z_h-axis parallel to the ρ^0-momentum and its y_h-axis along the cross product of beam and ρ^0 momentum. Finally, the sums in Eq. (3) are Bose symmetrized to account for the four indistinguishable final state configurations.

The simulations agree well with the two- and four-pion kinematic distributions. The mean ρ^0 reconstruction efficiency in the region $|y| < 1$ is about $21.9 \pm 0.2\%$, that for the ρ' approximately $6.5 \pm 0.5\%$. The efficiencies show no strong dependence on the z-position of the primary vertex or on the transverse momentum in the region of the coherent peak. However, due to the TPC acceptance, the efficiencies decrease to roughly 1 % for the ρ^0 and 0.1 % for the ρ', respectively, at $y = \pm 1$. The mass dependence of the ρ^0 efficiency is flat for masses above about 600 MeV/c^2 and decreases quickly for lower masses. The ρ' efficiency rises with mass, until it reaches a plateau at approximately 1500 MeV/c^2, so that the $\pi^+\pi^-\pi^+\pi^-$ mass peak in the uncorrected data is shifted towards larger masses (see the dashed curve in Fig. 5).

From the simulations the resolutions for p_T, y, and invariant mass of the selected pion pairs are estimated to be approximately 6 MeV/c, 0.009, and 5 MeV/c^2, respectively. The corresponding values for the four-pion combinations are 10 MeV/c, 0.006, and 10 MeV/c^2.

IV. RESULTS

The ratio of coherent ρ' and $\rho^0(770)$ production cross sections can be calculated from the respective acceptance-corrected yields which are determined from fits of the $\pi^+\pi^-\pi^+\pi^-$ and $\pi^+\pi^-$ invariant mass distributions, respectively.

Figure 5 shows the measured $\pi^+\pi^-\pi^+\pi^-$ invariant mass spectrum which exhibits a broad peak around 1540 MeV/c^2 indicating resonant ρ' production similar to what was seen in fixed-target photoproduction experiments [6–11]. This assumes that the peak is dominated by spin states with quantum numbers $J^{PC} = 1^{--}$. Contributions from other spin states cannot be ruled out, because in order to disentangle them a much larger data set would be required.

The data are fit in the range from 1 to 2.6 GeV/c^2 with a relativistic S-wave Breit-Wigner which is modified by the phenomenological Ross-Stodolsky factor [30] and which sits on top of a second order polynomial that parameterizes the remaining combinatorial background:

$$f_{4\pi}(m) = A \cdot \left(\frac{m_0}{m}\right)^n \cdot \frac{m_0^2\Gamma_0^2}{(m_0^2 - m^2)^2 + m_0^2\Gamma_0^2} + f_{\mathrm{BG}}(m) \tag{5}$$

Here m is the $\pi^+\pi^-\pi^+\pi^-$ invariant mass. The resonance mass m_0, the width Γ_0, and the exponent n are left as free parameters.

The background polynomial f_{BG} is fixed by fitting the invariant mass distribution of $+2$ or -2 charged four-prongs. Because at larger p_T the coherent cross section becomes negligible, the region $p_T > 250$ MeV/c is used to define the total amount of background by scaling the p_T distribution of the charged four-prongs, so that it matches that of the neutral four-prongs (cf. Fig. 2). This procedure treats incoherently produced $\pi^+\pi^-\pi^+\pi^-$ as background. The extracted scaling factor of 1.186 ± 0.054 — about half of the value estimated for the ρ^0 background (see below) — is applied to the background polynomial.

Fitting Eq. (5) to the data yields a resonance mass of 1540 ± 40 MeV/c^2, a width of 570 ± 60 MeV/c^2, and an exponent of $n = 2.4 \pm 0.7$. The values for mass and width, however, depend strongly on the choice of n. The

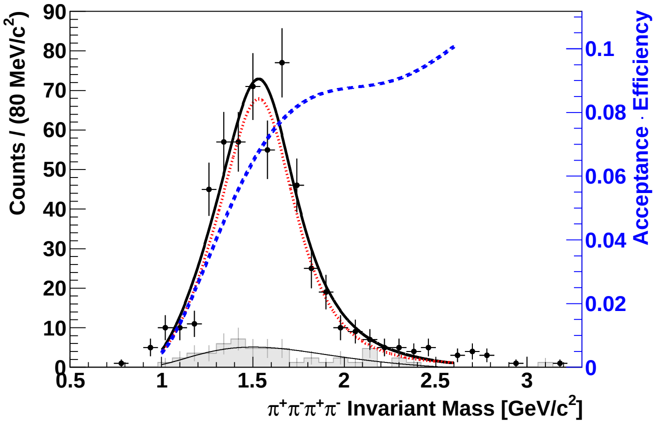

FIG. 5: (Color online) Invariant mass distribution of coherently produced $\pi^+\pi^-\pi^+\pi^-$: The filled circles are the measured points with the statistical errors, the gray filled histogram is the background estimated from charged four-prongs (cf. Fig. 2). The thick black line shows the fit of a modified S-wave Breit-Wigner on top of a second order polynomial background (thin black line; cf. Eq. (5)) taking into account the detector acceptance in the region $|y| < 1$ (rising dashed line). The dotted curve represents the signal curve without background.

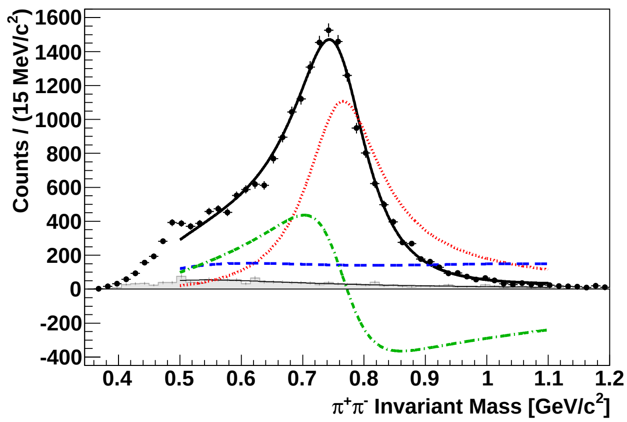

FIG. 6: (Color online) Invariant mass distribution of coherently produced $\pi^+\pi^-$ pairs. The filled circles are the measured points with statistical errors. The thick black line shows the fit taking into account the detector acceptance in the region $|y| < 1$. The non-interfering combinatorial background is represented by the thin black line, which is a fit to the like-sign invariant mass distribution scaled by a factor estimated from the p_T distribution (gray filled histogram). The dotted curve shows the Breit-Wigner without background, the dashed line the interfering background component that is assumed to be mass-independent. The dash-dotted curve is the Söding interference term of the two [31].

peak contains $N_{4\pi} = 9180 \pm 540$ events in the mass range from 1 to 2.6 GeV/c^2. As seen in Fig. 5 and also indicated by the χ^2/n.d.f. of the maximum likelihood fit of about 36/16, Eq. (5) does not describe the peak shape well. This is in accord with observations from other photoproduction experiments, which favor a description using two resonances in this mass region [9]. However, the low statistics of the data does not permit to extract the resonance and mixing parameters for a two-resonance scenario.

In both the background and the signal fit, the mass dependence of the reconstruction efficiency for $|y| < 1$ is taken into account (dashed curve in Fig. 5). The efficiency is parameterized by a fifth order polynomial determined by fitting the Monte Carlo data.

The $\rho^0(770)$ peak in the $\pi^+\pi^-$ invariant mass distribution of the selected two-prong data set is fit by a P-wave Breit-Wigner with mass-dependent width and Söding interference term [31] on top of a second order polynomial background as described in [13–15] (cf. Fig. 6). As in the ρ' case, the background polynomial is determined from a fit of the like-sign pair invariant mass distribution that is scaled up by a factor of 2.284 ± 0.050 which is extracted from the incoherent part of the p_T distribution. The fit gives a ρ^0 mass of 772.3 ± 1.2 MeV/c^2 and a width of 152.1 ± 1.9 MeV/c^2, in agreement with both the PDG data on ρ^0 photoproduction [4] and earlier results from photonuclear production [13–15]. As expected, modifications of the $\rho^0(770)$ properties that were measured in peripheral Au-Au collisions [32] and attributed to in-medium production are not observed in the current study. The Breit-Wigner peak contains $N_\rho = 55\,940 \pm 910$ events in the mass range from 500 to 1100 MeV/c^2. The χ^2/n.d.f. of the maximum likelihood fit is 115/36 which mainly reflects the fact that the fit function does not reproduce well either the high mass tail of the $\rho(770)$ or the low mass region. This mass region exhibits a peak from $K_s^0 \to \pi^+\pi^-$, where the kaons most likely come from photoproduced $\phi(1020)$.

Using the acceptance-corrected yields N_ρ and $N_{4\pi}$ for the $\rho^0(770)$ and the ρ', respectively, it is possible to calculate the cross section ratio for coherent ρ^0 and ρ' production which is accompanied by mutual nuclear excitation and where the ρ' decays into $\pi^+\pi^-\pi^+\pi^-$:

$$(6)\quad \frac{\sigma^{\mathrm{coh}}_{4\pi,xn\,xn}}{\sigma^{\mathrm{coh}}_{\rho,\,xn\,xn}} = \frac{\sigma^{\mathrm{coh}}_{\rho',\,xn\,xn} \cdot \mathcal{B}(\rho' \to \pi^+\pi^-\pi^+\pi^-)}{\sigma^{\mathrm{coh}}_{\rho,\,xn\,xn}} = \frac{N_{4\pi}}{N_\rho},$$

where $\mathcal{B}(\rho' \to \pi^+\pi^-\pi^+\pi^-)$ is the branching fraction of the ρ' into $\pi^+\pi^-\pi^+\pi^-$.

The cross section ratio does not depend strongly on rapidity and in the region $|y| < 1$ has a mean value of $16.4 \pm 1.0_{\mathrm{stat.}} \pm 5.2_{\mathrm{syst.}}$%. Based on the KN model [17] we estimate extrapolation factors to the full 4π solid angle of $1.8 \pm 0.1_{\mathrm{syst.}}$ for the ρ' and of $2.2 \pm 0.1_{\mathrm{syst.}}$ for the ρ^0, where the latter value is taken from [14]. With this extrapolation, the overall coherent cross section ratio is $13.4 \pm 0.8_{\mathrm{stat.}} \pm 4.4_{\mathrm{syst.}}$%. Using the measured cross section $\sigma^{\mathrm{coh}}_{\rho,\,xn\,xn}$ for coherent $\rho^0(770)$ production accompanied by mutual nuclear excitation of the beam particles from [14], the $\rho' \to \pi^+\pi^-\pi^+\pi^-$ production cross section can be calculated. The cross section within $|y| < 1$ is $\sigma^{\mathrm{coh}}_{4\pi,\,xn\,xn}(|y| < 1) = 2.4 \pm 0.2_{\mathrm{stat.}} \pm 0.8_{\mathrm{syst.}}$mb, the corresponding rapidity-integrated value is $\sigma^{\mathrm{coh}}_{4\pi,\,xn\,xn} = 4.3 \pm 0.3_{\mathrm{stat.}} \pm 1.5_{\mathrm{syst.}}$mb.

The influence of systematic effects on the cross section ratio was studied. The main source of systematic uncertainty comes from the model dependence of the angular distribution of the $\pi^+\pi^-\pi^+\pi^-$ used in the acceptance correction. This uncertainty is estimated to be 21 % by comparing to the cross section ratio obtained using an isotropic angular distribution in the Monte Carlo simulation. The uncertainty from the parameterization of the $\pi^+\pi^-$ S-wave in the four prong-decay model is about 11 % and is estimated by increasing the mass and/or width of the $f_0(600)$ Breit-Wigner to 600 MeV/c^2 and 1000 MeV/c^2, respectively. Additional systematic errors come from the event selection cuts (14 %), the background subtraction (10 %), as well as the invariant mass binning and the fit range (8 %). The systematic error associated with the particular choice of the fit function for the $\pi^+\pi^-\pi^+\pi^-$ invariant mass peak (cf. Eq. (5)) is estimated to be 9 % by trying to fit a non-relativistic Breit-Wigner and by fixing the value of the Ross-Stodolsky exponent in Eq. (5) to $n = 0$ and 4. The error for the extrapolation to the full 4π solid angle was estimated to be 6 % for the ρ^0 in [14] by comparing the KN [17] and the FSZ [18] models. The extrapolation factor depends on the photon-energy spectrum, which is well-known, and on the poorly known energy dependence of the photoproduction cross section. Because the KN model [17] describes the observed $\pi^+\pi^-\pi^+\pi^-$ rapidity distribution well, we assume that the ρ' production mechanism is not too different from that of the ρ^0 and assign the same systematic error of 6 %.

The measured cross section ratio cannot be compared directly to the ratio of the total exclusive coherent ρ' and ρ^0 cross sections of 14.2 % predicted by the FSZ model [18], because the branching fraction for $\rho' \to \pi^+\pi^-\pi^+\pi^-$ is not known. The ratio between the cross section for ρ' production accompanied by mutual Coulomb excitation, as measured here, and the exclusive coherent ρ' cross section, where the beam ions remain unchanged, should be similar to the one for the ρ^0. If in addition a 100 % branching fraction to the $\pi^+\pi^-\pi^+\pi^-$ final state is assumed, the measured cross section ratio agrees with the FSZ prediction. Under the same assumptions we can estimate, using the value for $\sigma^{\mathrm{coh}}_{\rho,\,0n\,0n}$ from [14] and the measured cross section ratio, the total exclusive coherent ρ' production cross section to be $\sigma^{\mathrm{coh}}_{\rho',\,0n\,0n} = 53 \pm 4_{\mathrm{stat.}} \pm 19_{\mathrm{syst.}}$mb. The value corresponding to the predicted cross section ratio is $56 \pm 3_{\mathrm{stat.}} \pm 8_{\mathrm{syst.}}$mb. These values are about half of the exclusive coherent ρ' cross section of 133 mb predicted by the FSZ model. On the other hand, this model predicts also ρ^0 cross section values roughly twice larger than observed by experiment [14].

In previous photoproduction experiments using carbon targets the ρ' was seen not only in the $\pi^+\pi^-\pi^+\pi^-$ decay mode, but also in $\pi^+\pi^-$ final states [11]. We do not observe a significant ρ' signal in the high mass region of the $m_{\pi^+\pi^-}$ spectrum as shown in Fig. 7. In order to suppress backgrounds, in particular cosmic rays, tighter cuts are applied: the rapidity is limited to $0.05 < |y| < 1$, the transverse momentum of the $\pi^+\pi^-$ pairs is required to be lower than 100 MeV/c, and the primary vertex is confined to $|z_{\mathrm{prim}}| < 70$ cm and $r_{\mathrm{prim}} < 8$ cm.

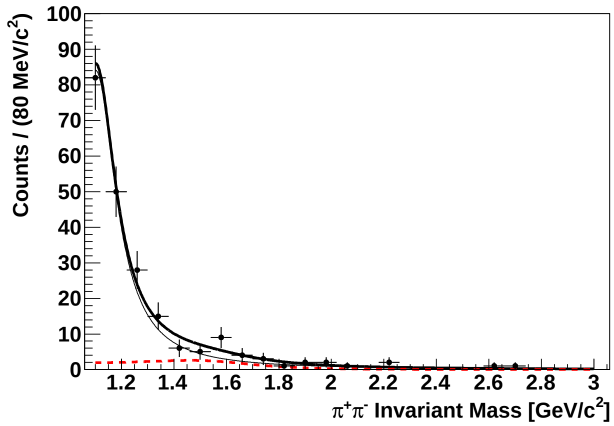

FIG. 7: (Color online) High mass region of the $m_{\pi^+\pi^-}$ spectrum with tighter cuts applied in order to suppress background: The filled circles are the measured values with statistical errors. No significant enhancement is seen in the region around 1540 MeV/c^2 where the $\pi^+\pi^-\pi^+\pi^-$ invariant mass spectrum exhibits a peak. The thick solid line shows the fit of a modified S-wave Breit-Wigner (cf. Eq. (5)) with parameters fixed to the values extracted from the fit of the $\pi^+\pi^-\pi^+\pi^-$ invariant mass distribution on top of an S-wave Breit-Wigner that describes the tail of the $\rho^0(770)$ (thin solid line) taking into account the detector acceptance. The dashed curve represents the signal curve without the ρ^0 tail.

The ρ' yield in the resulting $\pi^+\pi^-$ invariant mass spectrum is estimated by fitting the modified S-wave Breit-Wigner of Eq. (5) on top of an S-wave Breit-Wigner for the high-mass tail of the $\rho^0(770)$ in the mass range from 1.1 to 3 GeV/c^2. Assuming that the ρ' peak shape is the same in the $\pi^+\pi^-$ channel, we fixed mass, width, and exponent of the ρ' Breit-Wigner to the values obtained from the fit of the $\pi^+\pi^-\pi^+\pi^-$ invariant mass distribution. This gives an acceptance- and background-corrected ρ' yield of $N_{2\pi} = 110 \pm 90$ in the mass range from 1 to 2.6 GeV/c^2. $N_{2\pi}$ can be compared directly to the ρ' yield $N_{4\pi}$ in the $\pi^+\pi^-\pi^+\pi^-$ channel so that the ratio of the branching fractions of the ρ' to $\pi^+\pi^-$ and to $\pi^+\pi^-\pi^+\pi^-$ can be calculated:

$$R = \frac{\mathcal{B}(\rho' \to \pi^+\pi^-)}{\mathcal{B}(\rho' \to \pi^+\pi^-\pi^+\pi^-)} = \frac{N_{2\pi}}{N_{4\pi}} \tag{7}$$

Due to the low statistics, the measured value of $R = 0.012 \pm 0.010$ has a large uncertainty. The systematic error from neglecting the P-wave nature of the $\pi^+\pi^-$ decay by using a mass-independent resonance width in Eq. (5) is within the range of the statistical error. The corresponding upper limit of the ratio is $R < 2.5$ % at 90 % confidence level. This is an indication that, in the process measured here, R is smaller than the ratio of the total ρ' cross sections in the two- and four-pion channel on a carbon target which was measured to be $6.6 \pm 3.4\%$ [11].

V. CONCLUSIONS

We have observed diffractive photonuclear production of $\pi^+\pi^-\pi^+\pi^-$ final states in ultra-peripheral relativistic heavy ion collisions accompanied by mutual Coulomb excitation of the beam particles. The $\pi^+\pi^-\pi^+\pi^-$ invariant mass peak exhibits a broad peak around 1540 MeV/c^2. Under the assumption that the peak is dominated by spin states with $J^{PC} = 1^{--}$ this is consistent with the existing photoproduction data currently assigned to the $\rho^0(1700)$ by the PDG. No corresponding enhancement in the $\pi^+\pi^-$ invariant mass spectrum is found. The ratio of the branching fractions of the excited ρ^0 state to $\pi^+\pi^-$ and $\pi^+\pi^-\pi^+\pi^-$ final states is smaller than 2.5 % at 90 % confidence level. The coherent ρ' production cross section is $13.4 \pm 0.8_{\mathrm{stat.}} \pm 4.4_{\mathrm{syst.}}\%$ of that of the $\rho^0(770)$ meson.

Acknowledgments

We thank the RHIC Operations Group and RCF at BNL, the NERSC Center at LBNL and the Open Science Grid consortium for providing resources and support. This work was supported in part by the Offices of NP and HEP within the U.S. DOE Office of Science, the U.S. NSF, the Sloan Foundation, the DFG cluster of excellence 'Origin and Structure of the Universe', CNRS/IN2P3, STFC and EPSRC of the United Kingdom, FAPESP CNPq of Brazil, Ministry of Ed. and Sci. of the Russian Federation, NNSFC, CAS, MoST, and MoE of China, GA and MSMT of the Czech Republic, FOM and NWO of the Netherlands, DAE, DST, and CSIR of India, Polish Ministry of Sci. and Higher Ed., Korea Research Foundation, Ministry of Sci., Ed. and Sports of the Rep. Of Croatia, Russian Ministry of Sci. and Tech, and RosAtom of Russia.

[1] C. F. von Weizsäcker, Z. Phys. **88**, 612 (1934); E. J. Williams, Phys. Rev. **45**, 729 (1934).
[2] G. Baur, K. Hencken, D. Trautmann, S. Sadovsky, and Yu. Kharlov, Phys. Rept. **364**, 359 (2002); F. Krauss, M. Greiner, and G. Soff, Prog. Part. Nucl. Phys. **39**, 503 (1997); C. A. Bertulani, S. R. Klein, and J. Nystrand, Ann. Rev. Nucl. Part. Sci. **55**, 271 (2005); A. J. Baltz *et al.*, Phys. Rept. **458**, 1 (2008).
[3] A. J. Baltz, S. R. Klein, and J. Nystrand, Phys. Rev. Lett. **89**, 012301 (2002); G. Baur, K. Hencken, A. Aste, D. Trautmann, and S. R. Klein, Nucl. Phys. **A729**, 787 (2003).
[4] C. Amsler et al., Phys. Lett. **B667**, 1 (2008).
[5] T. Barnes, F. E. Close, P. R. Page, and E. S. Swanson, Phys. Rev. D **55**, 4157 (1997); F. E. Close and P. R. Page, Phys. Rev. D **56**, 1584 (1997); A. Donnachie and Yu. S. Kalashnikova, Phys. Rev. D **60**, 114011 (1999).
[6] H. H. Bingham *et al.*, Phys. Lett. **41B**, 635 (1972).
[7] P. Schacht, I. Derado, D. C. Fries, J. Park, and D. Yount, Nucl. Phys. **B81**, 205 (1974).
[8] G. Alexander, O. Benary, J. Gandsman, D. Lissauer, A. Levy, Y. Oren and L. M. Rosenstein, Phys. Lett. **57B**, 487 (1975).
[9] D. P. Barber *et al.*, Z. Phys. **C4**, 169 (1980).
[10] D. Aston *et al.*, Nucl. Phys. **B189**, 15 (1981); M. Atkinson *et al.*, Z. Phys. **C26**, 499 (1985).
[11] M. S. Atiya *et al.*, Phys. Rev. Lett. **43**, 1691 (1979).
[12] J. Adams *et al.*, Phys. Rev. C **70**, 031902(R) (2004).
[13] C. Adler *et al.*, Phys. Rev. Lett. **89**, 272302 (2002).
[14] B. I. Abelev *et al.*, Phys. Rev. C **77**, 034910 (2008).
[15] B. I. Abelev *et al.*, Phys. Rev. Lett. **102**, 112301 (2009).
[16] D. G. d'Enterria (for the PHENIX Collaboration), nucl-ex/0601001.
[17] S. R. Klein and J. Nystrand, Phys. Rev. C **60**, 014903 (1999).
[18] L. Frankfurt, M. Strikman and M. Zhalov, Phys. Lett. **B537**, 51 (2002); Phys. Rev. C **67**, 034901 (2003).
[19] V. P. Gonçalves and M. V. T. Machado, Eur. Phys. J. **C40**, 519 (2005).
[20] M. Anderson *et al.*, Nucl. Intrum. Methods **A499**, 659 (2003); **A499**, 679 (2003).
[21] F. S. Bieser *et al.*, Nucl. Intrum. Methods **A499**, 766 (2003).
[22] C. Adler *et al.*, Nucl. Intrum. Methods **A470**, 488 (2001).
[23] J. Kiryluk, Proceedings of 16th International Spin Physics Symposium (SPIN 2004), Trieste, Italy, Oct. 2004, hep-ex/0501072.
[24] A. Drees *et al.*, Proceedings of Particle Accelerator Conference (PAC 07), Albuquerque, New Mexico, June 2007.
[25] J. Nystrand and S. R. Klein, arXiv:nucl-ex/9811007v2; M. Kłusek, W. Schäfer, and A. Szczurek, Phys. Lett. **B674**, 92 (2009).
[26] GEANT 3.21 Package, CERN Program Library W5013.
[27] S. U. Chung and T. L. Trueman, Phys. Rev. D **11**, 633 (1975).
[28] F. von Hippel and C. Quigg, Phys. Rev. D **5**, 624 (1972).
[29] S. U. Chung and J. M. Friedrich, Phys. Rev. D **78**, 074027 (2008); S. U. Chung, Phys. Rev. D **57**, 431 (1998); **56**, 4419 (1997); **48**, 1225 (1993); 'Spin Formalisms', CERN Yellow Report 71-8 (1971).
[30] M. Ross and L. Stodolsky, Phys. Rev. **149**, 1172 (1966).
[31] P. Söding, Phys. Lett. **19**, 702 (1966); J. J. Sakurai, Ann. Phys. **11**, 1 (1960); T. H. Bauer *et al.*, Rev. Mod. Phys. **50**, 261 (1978).
[32] J. Adams *et al.*, Phys. Rev. Lett. **92**, 092301 (2004).